AN INVERSE FINITE ELEMENT ANALYSIS AND A PARAMETRIC STUDY OF SMALL PUNCH TESTS

A Thesis

by

ZHENZHEN XU

Submitted to the Office of Graduate Studies of
Texas A&M University
in partial fulfillment of the requirements for the degree of

MASTER OF SCIENCE

December 2011

Major Subject: Mechanical Engineering

An Inverse Finite Element Analysis and a Parametric Study of Small Punch Tests

AN INVERSE FINITE ELEMENT ANALYSIS AND A PARAMETRIC STUDY OF SMALL PUNCH TESTS

A Thesis

by

ZHENZHEN XU

Submitted to the Office of Graduate Studies of
Texas A&M University
in partial fulfillment of the requirements for the degree of

MASTER OF SCIENCE

Approved by:

Chair of Committee,	Xin-Lin Gao
Committee Members,	Xinghang Zhang
	Jun Kameoka
Head of Department,	Jerald Caton

December 2011

Major Subject: Mechanical Engineering

ABSTRACT

An Inverse Finite Element Analysis and a Parametric Study of Small Punch Tests.

(December 2011)

Zhenzhen Xu, B.S, Central South University, China

Chair of Advisory Committee: Dr. Xin-Lin Gao

Small punch test (SPT) has been widely used to evaluate in-service materials in nuclear fusion facilities. Early use of SPTs is largely based on empirical relations or curve fitting from experimental data, while recent applications of SPTs take advantage of finite element methods. In this study, an improved inverse finite element analysis procedure is proposed to obtain constitutive relations from load-displacement curves recorded in SPTs. In addition, a parametric study is performed to evaluate the effects of SPT parameters including friction coefficient, punch head diameter, sample thickness, specimen scale and boundary conditions.

The proposed inverse finite element (FE) method improves the accuracy of existing inverse FE methods, and the current parametric study provides a basis for the standardization of SPT procedures in the future.

DEDICATION

Dedicated to my family and teachers

ACKNOWLEDGEMENTS

I am heartily thankful to my advisor, Dr. Xin-Lin Gao, whose guidance, challenge, support and patience are felt from the initial admission to the final thesis research. His dedication, diligence, and persistence inspire me to always do my best in my graduate study and in my career development.

I would like to thank my committee members, Dr. Zhang, Dr. Kameoka, for their guidance and support.

Thanks also go to my friends and colleagues and the faculty and staff for making my time at Texas A&M University very enjoyable and memorable.

Finally, thanks to my family, for their encouragement, patience and love.

NOMENCLATURE

SPT	Small Punch Test
FE	Finite Element
FEM	Finite Element Method

TABLE OF CONTENTS

Page

LIST OF FIGURES

Page

LIST OF TABLES

Page

CHAPTER I

INTRODUCTION AND LITERATURE REVIEW

1.1 Introduction of Small Punch Test

Small punch test (SPT), also called miniaturized disk bending test, was invented in Japan and has become popular worldwide (Lucas, 1990). It is a powerful tool often used in nuclear engineering to evaluate the strength of an aged material in service.

1.1.1 Small Punch Test

Irradiation in a fast-neutron environment can cause significant ductility reduction for most alloys. To evaluate the safety of an in-service fusion reactor component, mechanical properties of the post-irradiation material should be determined. The driving force of SPTs has largely been the limited space in a reactor, gamma heating or fluency gradients in large specimen, and dose to personnel in post-irradiation testing (Corwin and Lucas, 1986). These limitations necessitate small specimen tests including small tensile tests, small pressurized tube tests, micro-hardness tests, and small punch test (ball, shear) (Husain et al., 2002). Table 1.1 provides a brief summary of various types of small specimen tests. Compared to conventional mechanical tests, small specimen tests provide mechanical properties with a much smaller volume of material.

Among these small specimen tests, a small punch test (SPT) can provide several types of mechanical properties: strength, ductility, ductile-brittle transition temperature, and fracture toughness with a small volume of material (Baik et al, 1983).

This thesis follows the style of Journal of the Mechanics and Physics of Solids.

This test overcomes the limitations of available material for conventional ASTM tests for small specimens.

Table 1.1 Small specimen tests and characteristics (Lucas, 1990)

Test	Specimen Volume (mm3)	Nature of Raw Data	Type of Properties	Nature of Analysis
Small Tensile	15	load-displacement	$\sigma = f(\varepsilon)$	direct
Pressurized Tube	350	diameter-time	creep rate, rupture time	direct
Micro hardness	1.7	load/area	strength, $\sigma = f(\varepsilon)$	empirical, semi-empirical
ball punch	1.7	load-displacement	ductility, strength, ductile-brittle transition temperature, fracture toughness	analytical, FEA, semi empirical
shear punch	1.7	load-displacement	strength,	analytical
bend	10	load-displacement	strength,	analytical
fracture	370	load-crack growth	fracture toughness	direct
impact	200	load-time-temperature	energy-absorbed strength	direct, analytical
fatigue	1000	load-cycles	S-N diagrams	direct

1.1.2 Apparatus

A schematic of a SPT is shown in Fig. 1.1. The test is essentially composed of a

center-loaded clamp disk with a ball punch head. As the punch head moves downward at a fixed speed, the load-displacement curve is recorded. Sample diameter (D_3), and thickness (t) are typically 3mm, 0.25mm, respectively. These geometric parameters are widely used, because they reflect not only the reduced size in nuclear power plant but also represent the standard sample size for transmission electron microscopy observations.

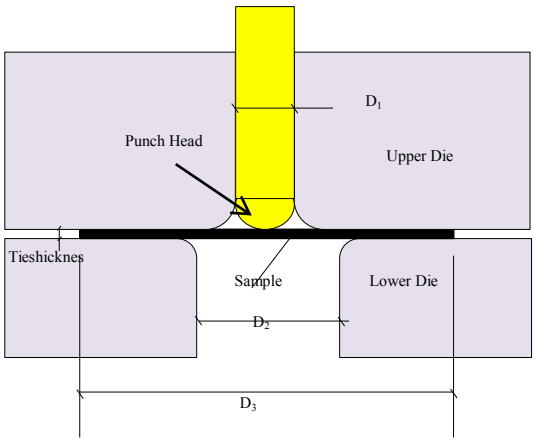

Fig. 1.1 Schematic of a small punch test set-up

Small specimens are cut from in-service component, but may have experienced some treatments such as weld, heat treatment, cold rolling, and intermediate annealing (Jung, 1996). For these applications, it is recommended that minimum changes of mechanical properties and microstructures, and treatment processes be recorded.

1.1.3 History of SPT

The earliest small punch test is also called miniaturized disk bend test, which was first proposed by Manahan et al. (1980). In their study, finite element analysis was used

to convert experimental data to stress strain curves. However, their finite element model is a 2-D model, and the mesh size is very large. Manahan (1981) suggested a theoretical method to obtain stress-strain curves from experimental load-displacement data.

Baik et al. (1986) developed a SPT to determine ductile-brittle transition temperatures, and proposed a transition temperature relation between a small specimen and a standard specimen. Based on experimental results Schwant et al. (1985) suggested an empirical equation to obtain value of the fracture toughness from the transition temperature.

Some work reported by Mao et al. (1987, 1991a, b) was conducted in Japan and employed SPTs to determine fracture toughness, yield strength and ultimate strength. Later Japan Atomic Energy Research Institute published a guide (Takahashi, 1988) for SPT experiment technology which is the first published standard for SPTs.

Fould et al. (1994) proposed an analytical method to determine fracture toughness from SPT load-displacement curve. This method improves the approach of Schwant et al. (1985) with only one test specimen required.

In Europe, SPT related studies started around 1992 and SPTs have been used under high temperature creep conditions. For example, Parker et al. (1995) proposed an empirical equation to determine creep fracture time from load-displacement curve.

European laboratories took a joint effort to develop small punch test method through participate the Copernicus project (Ding and Li, 2009). This project started in 1994 and ended in 1997, which was conducted by the Italian Electric Institute, and participated by research groups from Czech, Poland and Slovenia. In this project,

14MoV63 and X20CrMoV121 low alloy steel were tested at different temperatures, test results from SPT and standard samples were compared (Bicego, et al., 1995; Bicego et al., 1998; Bicego, et al., 2000; Dobes, et al., 1998; Milicka, 2004). Based on these studies, an empirical equation was proposed to determine creep fracture time from load-displacement curves.

From 2004 to 2006, the European Committee for Standardization organized workshops participated by 20 universities and research institutes to establish a standard for SPTs (European Committee for Standardization, 2007). This standard includes two parts: creep test and strength/toughness test.

1.2 Literature Review of Small Punch Test

SPTs have been used to extract a variety of material properties, including constitutive relations, creep, fracture toughness, ductile-brittle transition temperature, and damage.

1.2.1 Ductility

SPT was used to assess ductility of irradiated steels by Huang (Huang, et al. 1982). Experimental results were obtained from symmetric bending of a circular plate, and the load-line displacement at failure was converted to an effective failure strain. This approach has been employed to successfully identify ductility of steels. Doonley et al. (1981) investigated methods for obtaining plastic ductility directly from experiment curves directly. A planar isotropic plastic model is used to relate principle strains and the uniaxial ductility. As shown in their results, predicted values are in good agreement with measured results for a variety of materials.

SPT was also employed to extract material strength and ductility from load-displacement curves by Lucas et al. (1986) and Okada et al. (1988). Test parameters including ball diameter (d), hole size (D), and specimen thickness (t) were studied. Results showed that the yield force does not change with D or d, but increases with t; and that the maximum load increases with d and t.

1.2.2 Constitutive Relations

Since the experimental data from SPTs are in the form of load-displacement curves, the material properties cannot be directly obtained. Empirical relations or finite element analysis are used to determine material constitutive relations.

Manahan et al. (1981) developed a method to obtain material constitutive relations by using a 2-D finite element method. The analysis was able to identify various deformation regions of the material: initial elastic deformation, yield zone spreading through the specimen thickness and radius, material failure.

More recently, a pattern search optimization method has been used to access material constitutive relations. Egan et al. (2007) employed an inverse finite element method to analyze SPT data. A finite element deformation shape was described and compared with experimental results. By using an inverse optimization procedure, the true stress strain relationship was obtained.

Jerome and Tetsuo (2007) reported a new method for estimating the yield strength by measuring the elastic deformation energy. After the material was plastically deformed, unloading was done to release the elastic strain energy, which was used to estimate the yield stress.

1.2.3 Creep

SPT has also been applied to evaluate creep properties (e.g., Becker, et al. 1994; Butt, et al., 1996). Chen et al. (2010) developed a procedure to obtain creep properties using a finite element method. In their study, FE analysis was used to determine parameters involved in Norton's creep power law.

Zhou et al. (2010) carried out small punch creep tests for SUS304 and CR5Mo materials. A modified K-R creep damage constitutive relation was proposed and based on the FE simulation results.

1.2.4 Fracture Toughness

Efforts have been made to extract fracture and impact data from SPT results. Baik et al. (1986) conducted SPTs using ferritic coupon specimens over a range of temperatures. From the load-displacement curve the energy absorbed by the specimen was obtained. The absorbed energy shows a transition from low to high with increasing temperature, which indicates a fracture mode transition from brittle to ductile. The mid-point of the two absorbed energy extremes is defined as transition temperature.

Mao et al. (1991b) has attempted to access fracture toughness in ductile materials using SPTs. They determined an effective fracture strain with initial toughness. Strains near cracks of failed specimens were evaluated to determine the effective fracture strain. However this technique is only valid for certain steels, and a more general needs to be developed. An empirical relation was proposed based on the plasticity theory, which correlates the punch deflection at fracture with the effective fracture strain.

1.2 5 Damage

A widely used damage model for metallic material is the Gurson-Tvergaard-Needleman (GTN) plastic damage model. The GTN damage model was first proposed by Gurson (1977), and later modified by Tvergaard (1981) and Needleman and Tvergaard (1984).

Aberdroth and Kuna (2006) proposed a method to identify damage and fracture properties of ductile materials. The damage model was implemented in their finite element model, and simulated load-displacement relations were compared with the experimental results. A systematic variation of material parameters was done to train neutral networks. The criterion was to achieve a minimum error between the experimental and FE load-displacement curves. Hu and Ling (2009) evaluated mechanical properties of Zirconium using SPTs and FE analysis where the GTN damage model was implemented.

1.3 Finite Element Analysis and Small Punch Test

The major advantage of SPT is that it requires a small volume of material, which is good for in-service facilities. However a main disadvantage is that mechanical properties of the material cannot be obtained directly. In early studies of SPTs, mechanical properties were determined using empirical relations and curve fitting analysis experiment data. In recent investigation, inverse finite element methods have been employed in most SPT analysis procedures, and experiment load-displacement curves are fitted by adjusting input of material parameters in the finite element model. So that the output of FE model will best fit the experimental curves.

Since the first FE analysis of SPT was published by Manahan (1981), a lot progress has been made by linking SPTs with FE modeling (Lucas et al., 2007).

Abendroth et al. (2006) proposed a method for identifying deformation, damage and fracture properties of ductile materials. FEM simulations were carried out to establish a data base which serves to train a neural network (Fig. 1.2).

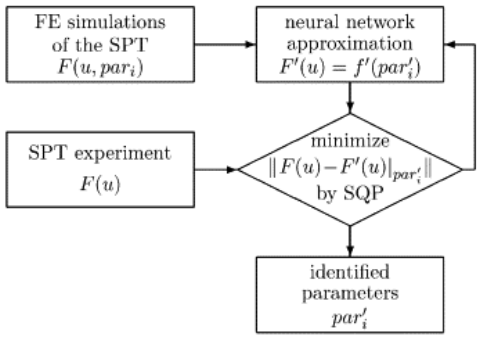

Fig. 1.2 Schematic of the identification procedure (Abendroth et al., 2006)

An inverse finite element procedure is proposed by Husain (2004) to access constitutive relations. The experimental load-displacement curve was divided into several pieces, and the curve fitting was done by piece from the beginning of the curve.

Egan et al. (2007) also carried out a similar study that includes experiments, sensitivity analysis, and optimization. His results show small variations in material properties affected the deformation.

Dymacek and Milicka (2008) created two FEM models, one including friction and the other one without friction. The simulation results showed that the friction

coefficient is a key factor of the SPT model.

Campitelli (2009) investigated the post-yield behavior of the SPT specimen with FEM simulations, and proposed a new calibration procedure to determine the yield stress of the specimen material.

Pathak et al. (2009) studied the influence of material parameters including: fillet radius, ball diameter, sample thickness, yield stress, and friction in a FE analysis. Their results showed that penetration is larger for larger fillet radius. Also, the sample deforms at a higher peak load if the punch ball diameter increases, which the depth of penetration is unrelated to the ball size. Moreover, the peak load increases with the increase of the sample thickness, while the penetration is the same in different samples. In addition, the peak loading and the corresponding stroke will increase with the increase in friction.

1.4 Conclusion

Although many studies have been conducted to extract mechanical properties from SPT data, the inverse FE methods used in these studies have not been fully developed. This includes the determination of yield stress and the uniqueness of material plastic behavior. Also, variations of test geometrical parameters of SPT result in different load-displacement curves, which also limit the efficiency of SPT.

In this study, a new method to obtain constitutive relations from SPT data is proposed base on an inverse FE method (Husain, 2004). The yield stress of the specimen material is determined in the FEM analysis, and the material post-yield behavior is characterized by curve fitting experimental load-displacement curves. Parameters including friction coefficient, sample thickness, punch head size and boundary

conditions are evaluated in the FEM simulations.

CHAPTER II

INVERSE FINITE ELEMENT METHOD FOR CONSTITUTIVE RELATIONS USING SMALL PUNCH TEST

2.1 Introduction

Inverse problems involve the determination of unknown causes of known consequences. An inverse finite element method for a SPT utilizes the experimentally obtained load-displacement curve as a known consequence. In conventional finite element simulations, the output is determined from a given set of initial conditions. Inverse simulation is defined as a reverse of this procedure, where the output is predefined and an inverse simulation algorithm allows one to determine the corresponding input parameters.

2.1.1 Application of Inverse Finite Element Method for Small Punch Test

Small punch test is used to measure mechanical properties of a material employing a small specimen extracted from a large in-service component. This testing method has been used to estimate ductile-to-brittle transition temperatures, fracture toughness, yield stress, and tensile stress. An inverse finite element method can be applied to the small punch test determine mechanical behavior of a material.

2.1.2 Procedure of Inverse Finite Element Method and Disadvantage

Finite element method has been successfully applied to predicting stress-strain curve based on load-displacement curve measured using SPTs. The objective of an inverse finite element method for a small punch test is to determine unknown material

parameters from experiment results.

In a conventional finite element method, the following input parameters are given: elastic modulus, yield stress, and stress-strain curve from a uniaxial test. While in an inverse FE method, these parameters are evaluated as output values.

The procedure of an inverse finite element method in a SPT can be described as follows (Husain, 2004):

1. The load-displacement curve from the SPT is divided into several segments (see Fig. 2.1), and an inverse FE analysis is used to obtain the corresponding constitutive relation that matches each segment, in the experimental load-displacement curve.

2. For the first (linear) segment P1, the elastic modulus is obtained in the inverse FEM analysis. It starts with an assumed value of elastic modulus, which is then increased or decreased to match the experiment curve. The yield stress equals the von-Mises stress at the end of the first segment.

3. For the second segment, the punch load P2 is input into the FE model. At this time the disk deforms plastically, and the plastic strain is adjusted to match the experimental load-displacement curve from the SPT. The final value of the von-Mises stress and the equivalent plastic strain will be those of the second data point.

4. Similarly, the nth segment of the experimental load-displacement curve can be analyzed.

5. Finally, the mechanical behavior of the specimen is determined, with the elastic modulus, yield stress, and uniaxial true stress-strain curve obtained.

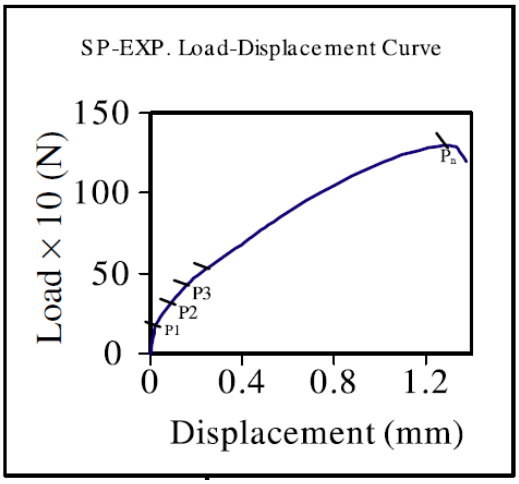

Fig. 2.1 Load-displacement curve from a small punch test (Husain et al., 2004)

One problem with this analysis method is that the assumed linearity in the first segment does not necessarily mean the disk deforms elastically. To address this issue, an improved method is proposed below.

2.2 Improved Inverse Finite Element Method

For the existing inverse finite element method introduced in Section 2.1, the first segment is treated as elastic, from which the elastic modulus and yield stress are obtained.

In this study, we propose an improved method, which is schematically shown in Fig. 2.2). In the first segment only the elastic modulus is input as a material property, and no plastic deformation is present that the disk has not yielded. A range of elastic values are input in the FE analysis at very small deflections. To ensure that the load-displacement curve from FE analysis is very close to the experimental curve from the SPT, the root square standard deviation is calculated to evaluate the accuracy of modulus value. The results must show difference with the experimental curves since no plastic deformation is present. Then, a deviate point of yield point will come up, which means that the sample disk starts to yield. The corresponding yield point with yield stress and yield strain is obtained from analysis, it is also the start iterate point of next segment analysis. This procedure is illustrated in Section 2.4.

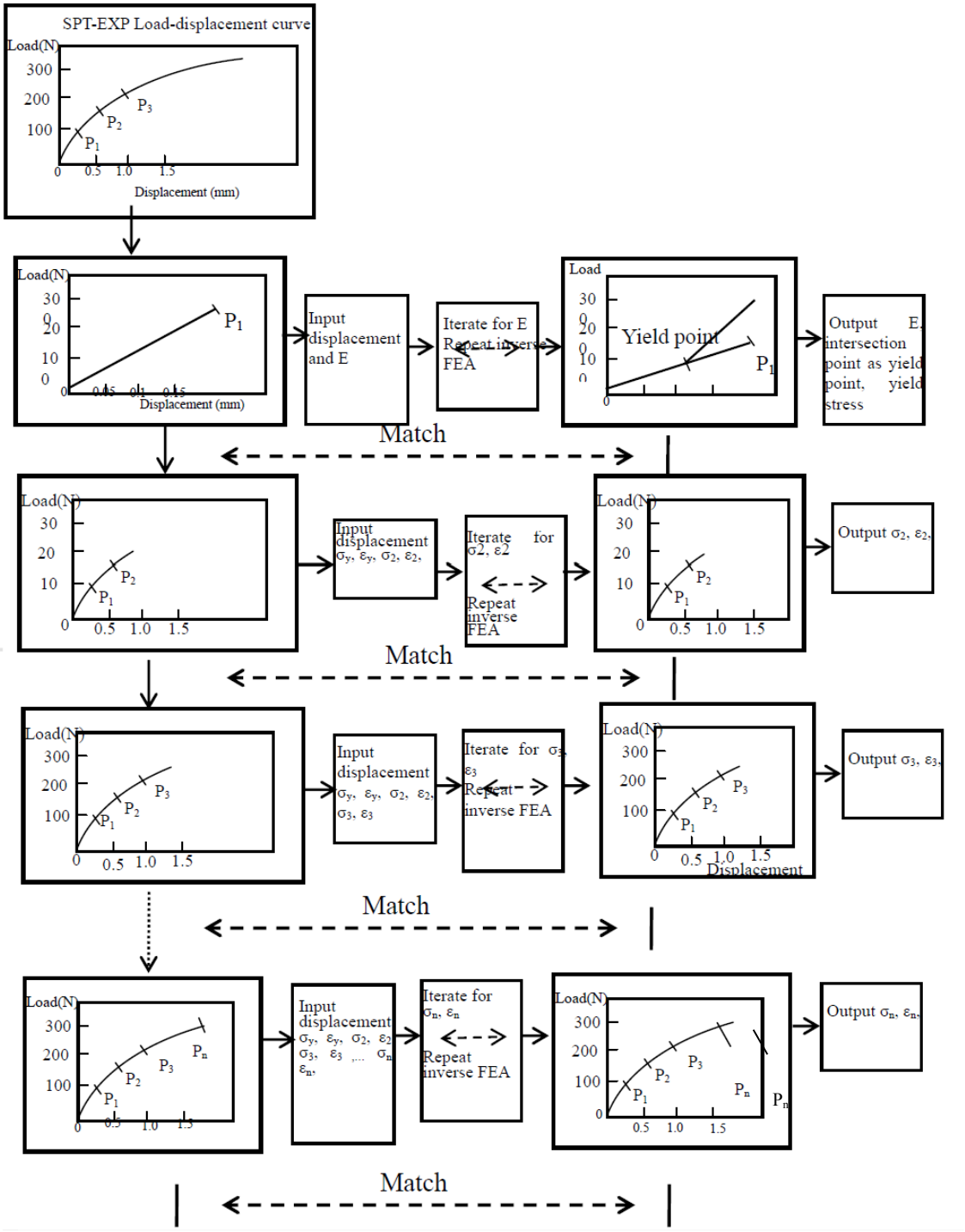

Fig. 2.2 Flow chart of the improve inverse finite element method

2.3 Finite Element Model for SPT

This simulation study is based on the experimental work by Guan et al. (2011) (Fig. 2.3 schematically shows the experimental set up). A quarter model is used in the simulations procedure, due to symmetry the sample disk diameter and thickness are 10mm, 0.5 mm, respectively, and the punch head diameter is 2.5mm. The FE model is shown in Fig.2.4-2.5. The disk outer part is clamped between upper and lower die. In the FE model, the clamped part is fixed in all 3 directions. The load case is applied through the punch head that moves downward.

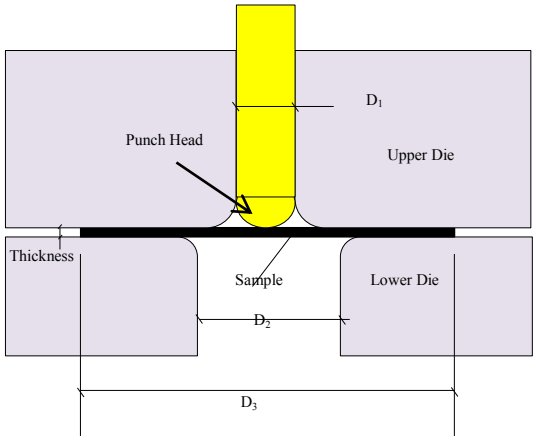

Fig. 2.3 Schematic illustration of a small punch test

The element used to describe the sample disk is C3D8R in ABAQUS, which is a three-dimensional, hexahedral, eight-node, solid element. This element can be used for linear and nonlinear problems involving contact, plasticity and large deformations. The C3D8R element has three translational degrees of freedoms at each node U_1, U_2, U_3,

and, as the element output, the stress components: σ_{11}, σ_{22}, σ_{33}, τ_{12}, τ_{23}, τ_{13}.

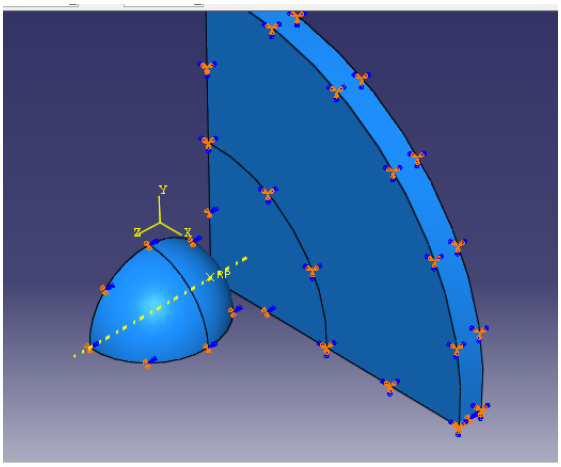

Fig. 2.4 Boundary condition of the finite element model

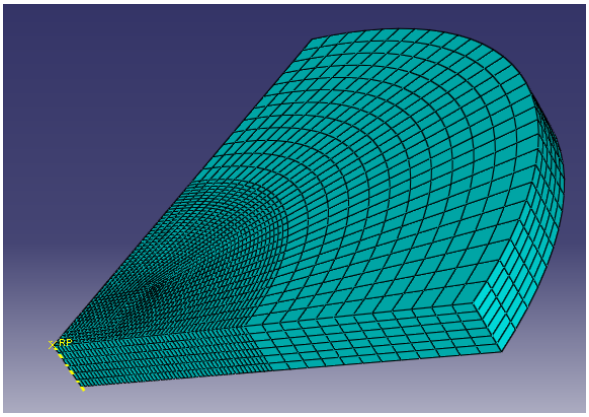

Fig. 2.5 Mesh of the finite element model

2.4 Elastic Modulus and Yield Stress

The first step is to determine the elastic modulus. As indicated in Fig.2.7, in this step the input for the material property in the FE model is the elastic modulus only and no plasticity is considered. The elastic modulus is input as 200GPa, 210GPa, and 220GPa, respectively. Since the deflection of the dish is very small (less than 0.005mm), the punch force needed for this deflection is also small.

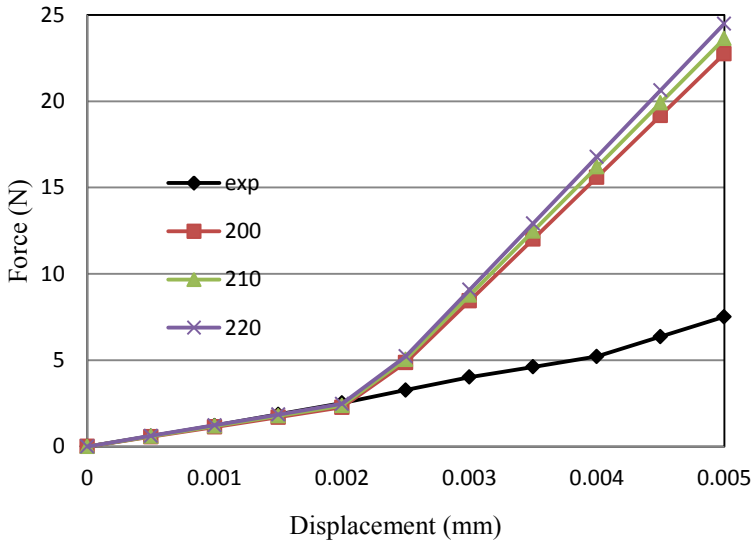

Fig. 2.6 Determination of the elastic modulus and yield stress

While the disk material yields in the SPT, the FE simulation in the first step does not consider material yielding. At the beginning of the deformation, the sample disk material is elastically deformed, and thus from the SPT and the FE simulation overlap. By comparing the two load-displacement curves, the corresponding punch head

displacement at the intersection point can be identified as the displacement where the sample material starts to yield. The von-Mises stress at this point will be the yield stress. Since the sample material has just started yielding, the plastic strain is 0.

In order to characterize the elastic modulus, the root mean square deviation (RMSD) is calculated using Eq. 2.1, with the result shown in Table 2.1. From Table 2.1, it can be concluded that the 220GPa with the smallest RMSD of can be taken to be the disk material.

$$\mathrm{RMSD} = \sqrt{(\sum_{i=1}^{n}(x_{1,i} - x_{2,i})^2)/n} \qquad \text{(Eq.2.1)}$$

Table 2.1 Elastic modulus and RMSD of 40CrNi2Mo alloy steel

Elastic Modulus	200GPa	210GPa	220GPa	250GPa
RMSD	0.112	0.061	0.016	0.396

As shown in Fig. 2.6, the intersection point of the SPT curve and the FEM simulation curve with the elastic modulus of 220MPa is the yield point, where the punch head displacement is 0.002mm, the von-Mises stress is 336.8MPa, and the true strain is 0.15%. This yielding point is also the starting point of iterative steps.

Hence, the elastic modulus and yield stress of the sample material have been determined.

2.5 Plastic Behavior of the Material

Plastic behavior of the disk material can be obtained from curve fitting the

experimental data and simulation results. The load-displacement curve of 40CrNi2Mo alloy steel measured using a SPT (Guan, 2011) is divided into linear pieces (see Fig. 2.7): P_1, P_2, P_3, P_4, …, P_{14}, P_{15}.

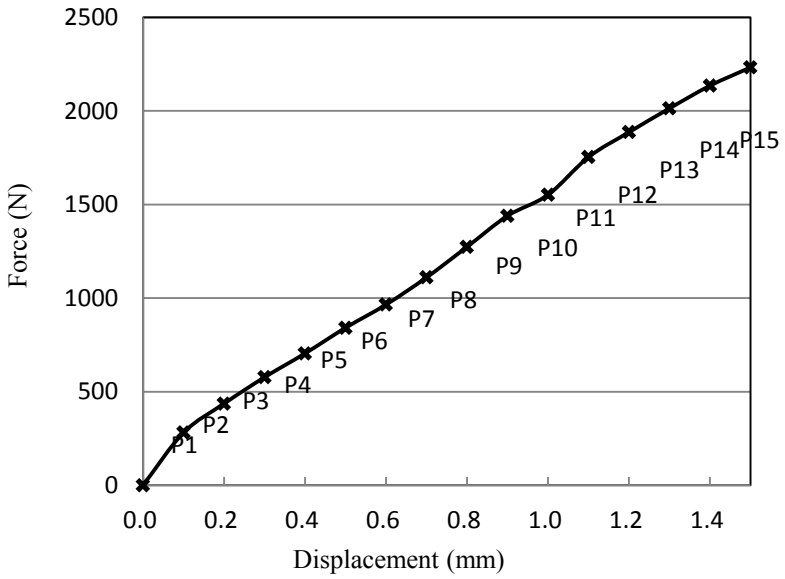

Fig. 2.7 Load-displacement curve of 40CrNi2Mo alloy steel (Guan et al., 2011)

2.5.1 Strain Estimate for the First Iterative Step

For the first segment $0P_1$, the displacement ranges from 0.0 to 0.1 mm, the elastic modulus, yield stress and yield strain are 220MPa, 336.8MPa, 0.15% respectively. In order to get the start stress-strain parameters, estimation is performed based on the following sample disk deformation (see Fig. 2.8).

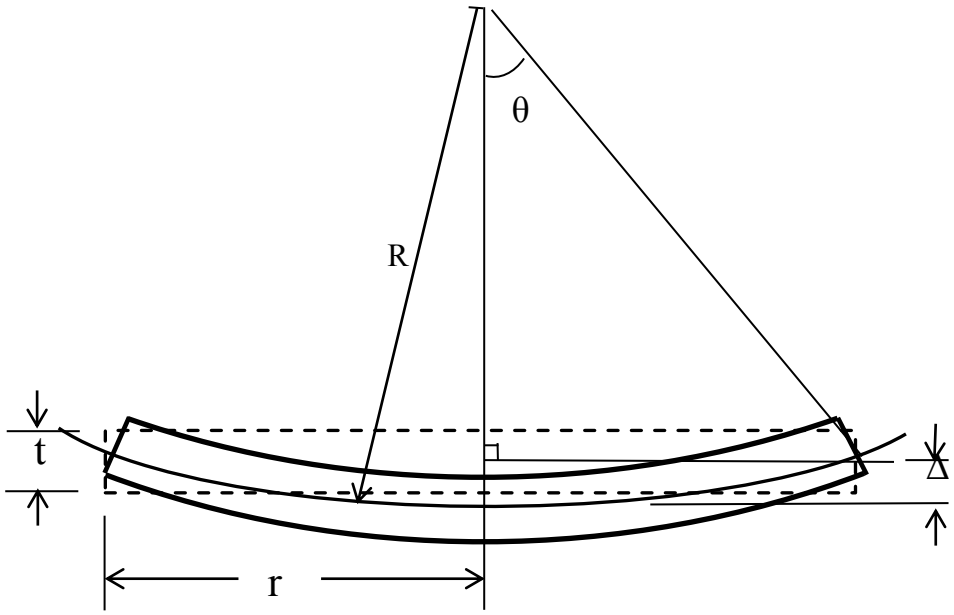

Fig. 2.8 Estimate of the first step displacement

Here R is the radius of the mid plane of the sample disk in the deformed configuration, r is the radius of the disk (in this test r equals 1.25mm), t is the sample thickness which equals 0.5 mm here, θ is the half of the angle of the bending curve, and Δ is the punch head displacement. From the triangle in the shadow, it follows that:

$$R^2 = r^2 + (R - \Delta)^2 , \tag{2.2}$$

$$R = \frac{r^2 - \Delta^2}{2\Delta}. \tag{2.3}$$

Note that at the beginning of the deformation Δ is very small and r = 1.25mm. Then Eq. 2.3 can be rewritten as:

$$R = \frac{0.78}{\Delta}. \tag{2.4}$$

The maximum strain ε in the disk is located at the midpoint of the upper and lower surface, which can be obtained as:

$$\varepsilon = \frac{\left(R+\frac{t}{2}\right)\theta - r}{r} = \frac{t\theta}{2r} = \frac{t}{2r} \tag{2.5}$$

Substituting Eq. (2.4) into Eq. (2.5), gives:

$$\varepsilon = \frac{\mathrm{t}}{2\mathrm{R}} = 0.32\Delta \tag{2.6}$$

2.5.2 Iterative Steps in the Inverse FE Simulation

At small deformations, the maximum strain and punch head displacement satisfy the relation obtained in Eq. (2.6) which can be used to determine the iterative step input of material plastic stress-strain parameters in the FE analysis.

1. For the first step, the punch head displacement is 0.1 mm, and the corresponding strain estimated from Eq. (2.6) is 0.032. The input strain in the FE simulation is taken to be two times that of the estimated strain. The input parameters in the FE simulation are the elastic modulus of 220GPa, yield stress of 336.8MPa, and the plastic strain 0. The load-displacement curve from the FE model with these input parameters are shown in Fig. 2.10. Also, the stress at $\varepsilon = 0.064$ is taken to be 800 MPa.

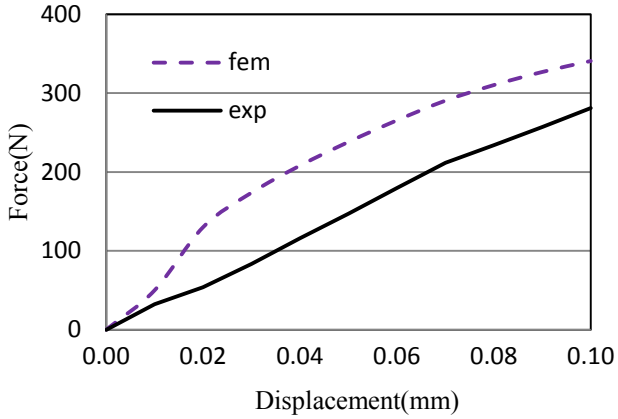

Fig. 2.9 FE simulation results with σ = 800 MPa at ε = 0.064

From Fig. 2.9, it is apparent that the FE simulation result is larger than the experimental value, with a difference being at about 50%. Based on this observation, the input stress is decreased to 720MPa at strain 0.064, in the next iterative step. The new result is shown in Fig. 2.10.

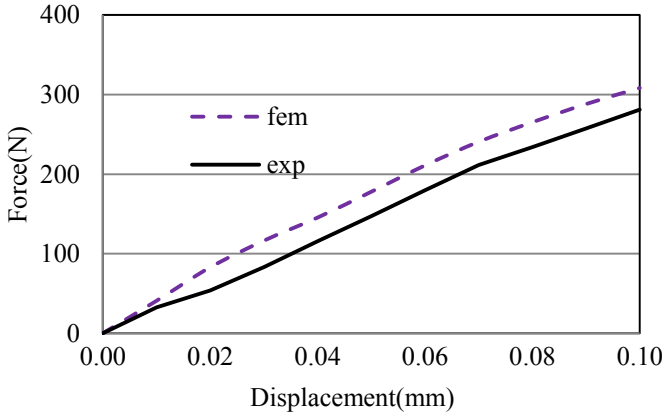

Fig. 2.10 FE simulation results with σ = 720 MPa at ε = 0.064

The two set of results shown in Fig.2.10 are correlated with a RMSD of 11%, which is larger than the tolerance 5%. Hence, the iteration proceed continues with the stress further reduced to 680MPa.

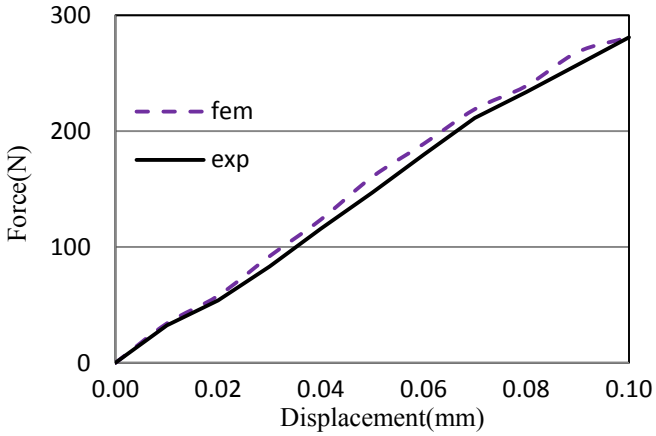

Fig. 2.11 FE simulation results with σ = 680 MPa at ε = 0.064

From Fig. 2.11, it is seen that the FE simulation results are very close to those of the experiment data with RMSD of this curve being 2.8%. As the curve fitting tolerance is 5%, satisfactory results have been obtained. In the FE simulations, the maximum von-Mises stress is 640MPa, and the strain is 0.058. These values will be used to plot the uniaxial true stress-true strain curve.

2. After the first step, the next iterative step uses the following input parameters: $E = 220\text{GPa}$, $\sigma_{0.064} = 640MPa$. The second input true stress is taken to be $\sigma = 1200MPa$, at $\varepsilon = 0.1$. The FE simulation results for the first round are shown in Fig. 2.12.

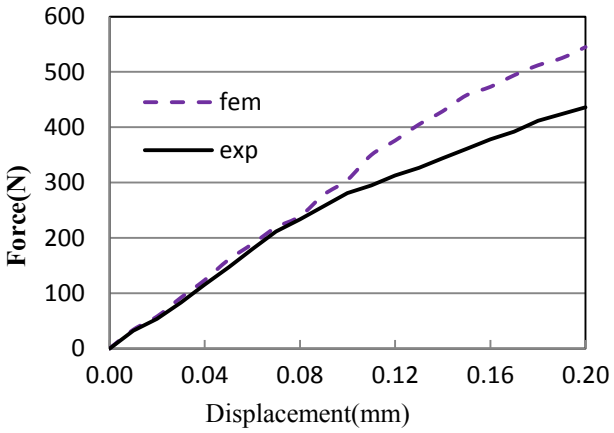

Fig. 2.12 FE simulation results with σ = 1200 MPa at ε = 0.1

The RMSD for this curve fitting from 0.1 mm to 0.2 mm shown in Fig. 2.13 is 16% which is much larger than the tolerance 5%. Hence the stress is decrease to 1150 at $\varepsilon = 0.1$.

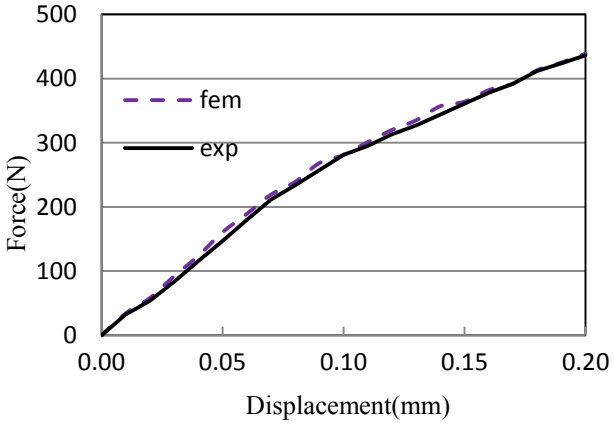

Fig. 2.13 FE simulation results with σ = 1050 MPa at ε = 0.1

With $\sigma_{0.1} = 1050MPa$ input in the FE simulation, the resulting load-displacement segment shows a good fitting with the experimental curve, with the RMSD

being at 1.6%.

3. The iterative steps continue until the true strain reaches fracture strain of 0.4936 (Guan, 2011). The FE simulation results at various iterative steps are shown in Fig. 2.14-Fig 2.16. When the punch head displacement is 0.5mm in the disk, material strain reach 0.4936 which is fracture stain. That is when the iteration ends. The true stress-strain curve for the disk material shown in Fig. 2.17.

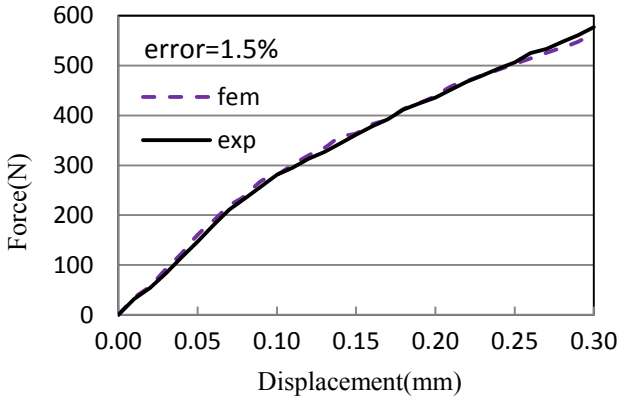

Fig. 2.14 FE simulation results with σ = 1520 MPa at ε = 0.35

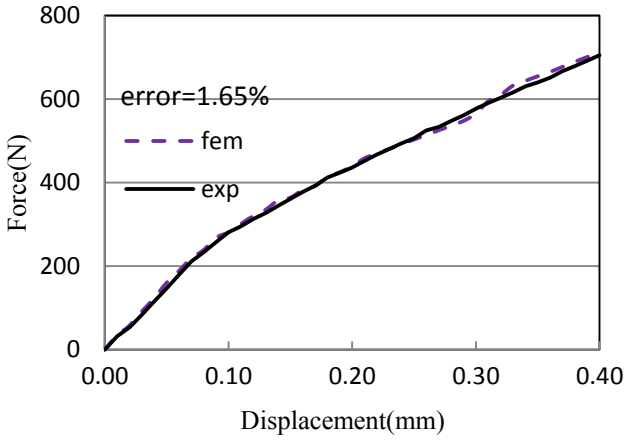

Fig. 2.15 FE simulation results with σ = 1650 MPa at ε = 0.45

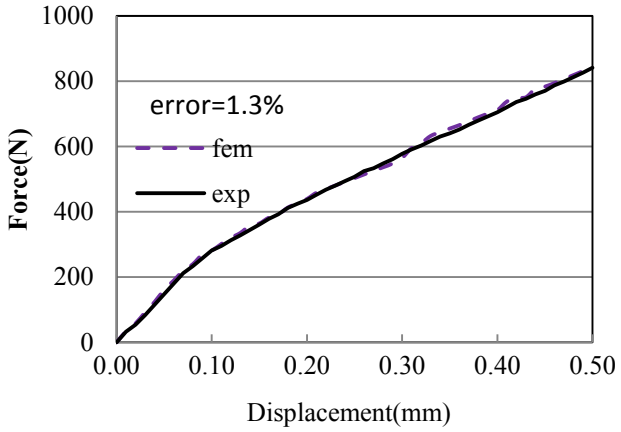

Fig. 2.16 FE simulation results with σ = 1720 MPa at ε = 0.49

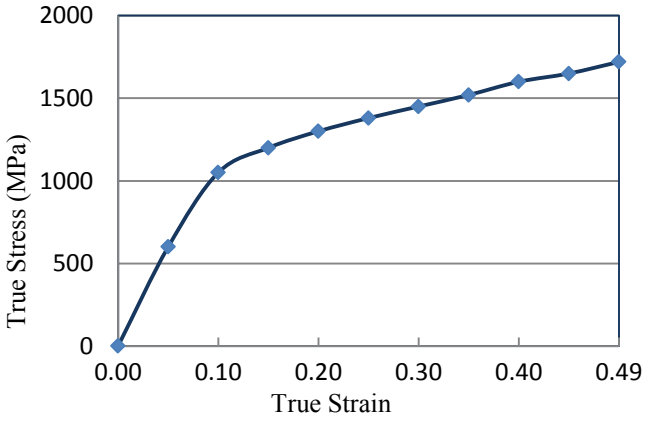

Fig. 2.17 True stress-strain curve of 40CrNi2Mo alloy steel from the inverse FE analysis of the SPT

2.6 Results for Other Materials

Base on the SPTs of 1.25Cr0.5Mo and 23CrNiMoWV alloy steels (Guan et al., 2011), the true stress-strain curves of these two materials have also been simulated by

using the current inverse FE model.

1. 1.25Cr0.5Mo alloy steel.

Table 2.2 Elastic modulus and RMSD of 1.25Cr0.5Mo alloy steel

Elastic Modulus	200 GPa	210GPa	220GPa	250GPa
RMSD	0.147	0.101	0.158	0.884

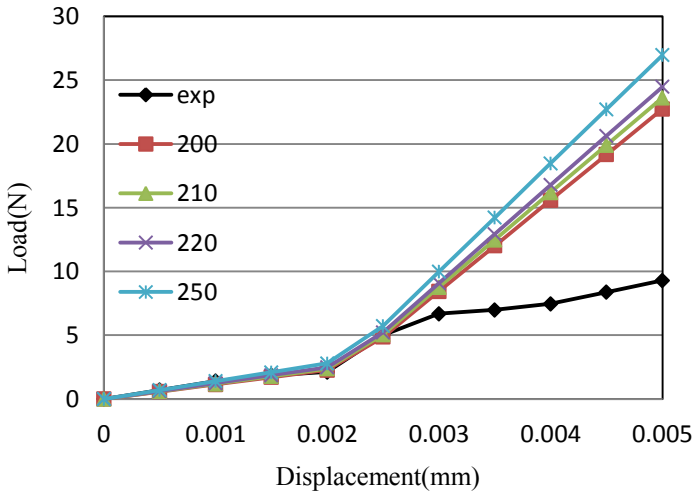

Fig. 2.18 1.25Cr0.5Mo alloy steel elastic modulus and yield stress

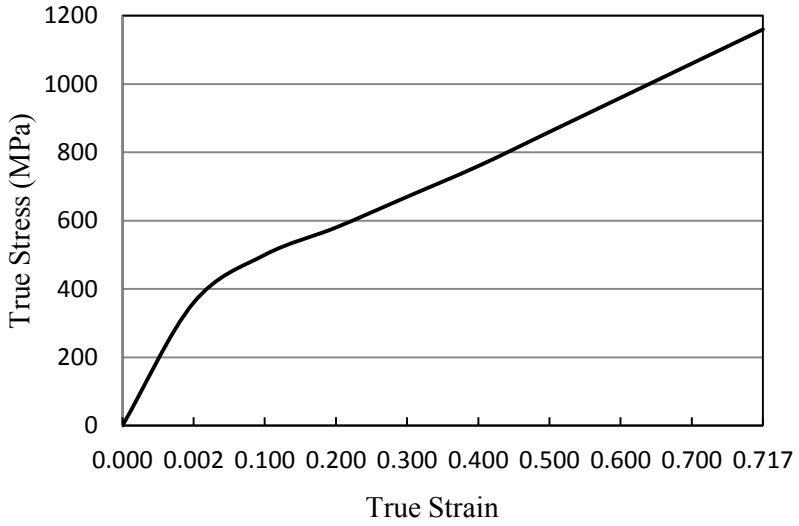

Fig. 2.19 True stress-strain relation of the 1.25Cr0.5Mo alloy steel

As shown in Fig. 2.18 and Table 2.2, the elastic modulus for the 1.25Cr0.5Mo alloy steel is found to be 210GPa, with the smallest RMSD of 0.101. Also, it is determined that yield stress is 470MPa and the yield strain is 2.24%. The true stress-strain curve of the material predicted by the current inverse FE model is shown in Fig. 2.19, where the fracture strain is seen to be 0.717.

2. 23CrNiMoWV alloy steel.

Table 2.3 Elastic modulus and RMSD of 23CrNiMoWV alloy steel

Elastic Modulus	200 GPa	210 GPa	220GPa	250GPa
RMSD	0.06	0.05	0.09	0.42

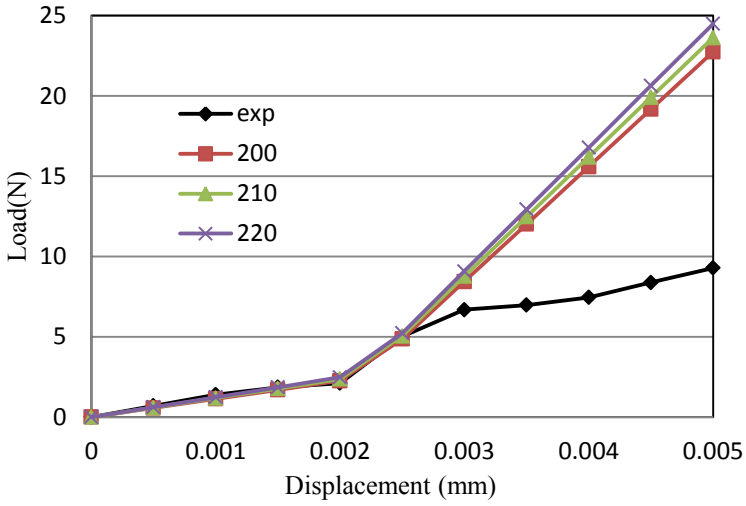

Fig. 2.20 23CrNiMoWV alloy steel elastic modulus and yield stress

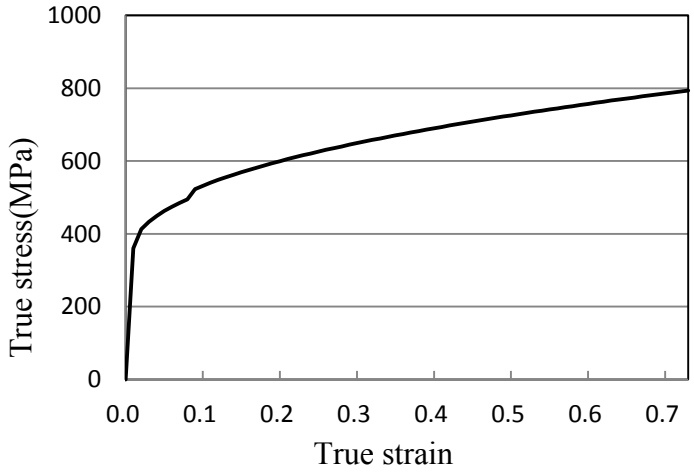

Fig. 2.21 True stress-strain curve of the 23CrNiMoWV alloy steel

As shown in Fig. 2.20 and Table 2.3, the elastic modulus for the 23CrNiMoWV alloy steel is found to be 210GPa, with the smallest RMSD of 0.05. Also, the yield stress is determined to be 470MPa, and the yield strain is 2.24%. The true stress-strain curve of

material predicted by the current inverse FE model is shown in Fig. 2.21. where the fracture strain is 0.717.

2.7 Conclusion

In this chapter, an improved inverse FE method for SPT is proposed and applied to predict the true stress-strain curve of three different materials 40CrNi2Mo, 1.25Cr0.5Mo, 23CrNiMoWV alloy steels, on the load-displacement curves measured using SPTs.

The constitutive relations of the long-term-service low alloy steels 40CrNi2Mo, 1.25Cr0.5Mo, 23CrNiMoWV are characterized using the proposed inverse FE method.

CHAPTER III

PARAMETRIC STUDY OF SMALL PUNCH TESTS

Although small punch tests have long been used in evaluating in-service power plant facilities, no standard has been established for such tests. For a widely and convenient use of small punch tests, it is essential to standardize the test technique. To this end, the effect of test parameters should be well understood.

In this chapter, the inverse finite element model developed in Chapter II is modified to analyze the effect of parameters including: friction coefficient, specimen thickness, punch head size, and boundary conditions. The experimental data from the SPT of 40CrNi2Mo alloy steel is selected in this study.

3.1 Friction Coefficient

During the specimen preparation, different surface treatment condition will result in variations in punch head force. In the analysis of the friction coefficient effect, the inverse FE model developed in Chapter II (see Fig. 3.1) is directly used. Friction coefficient is adjusted to be 0, 0.05 and 0.1 respectively, in the analysis. The major results from the FE simulations are displayed in Figs. 3.2 and 3.3.

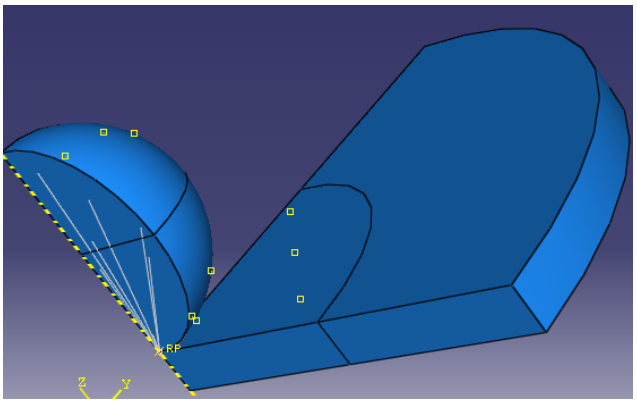

Fig. 3.1 FE model for the friction coefficient effect analysis

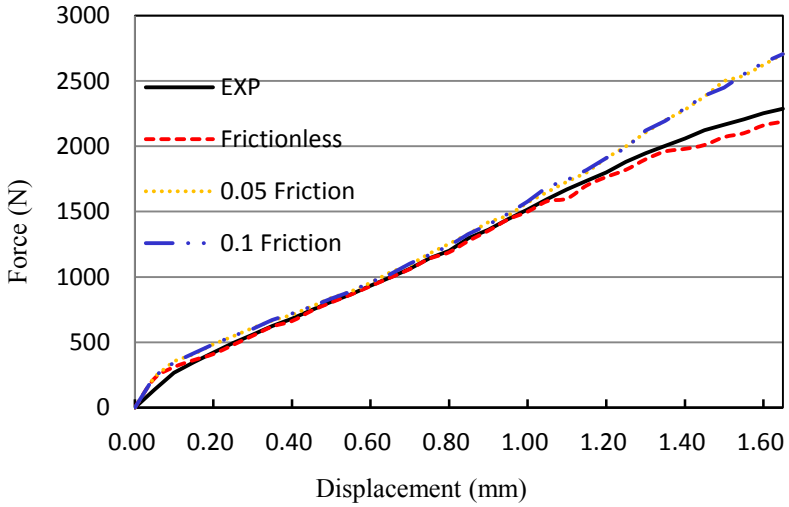

Fig. 3.2 Comparison of the FE simulation results

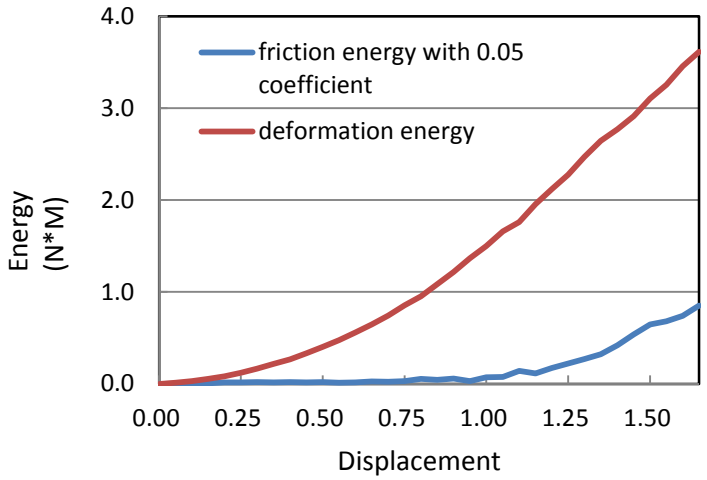

Fig. 3.3 Comparison of the friction energy and deformation energy

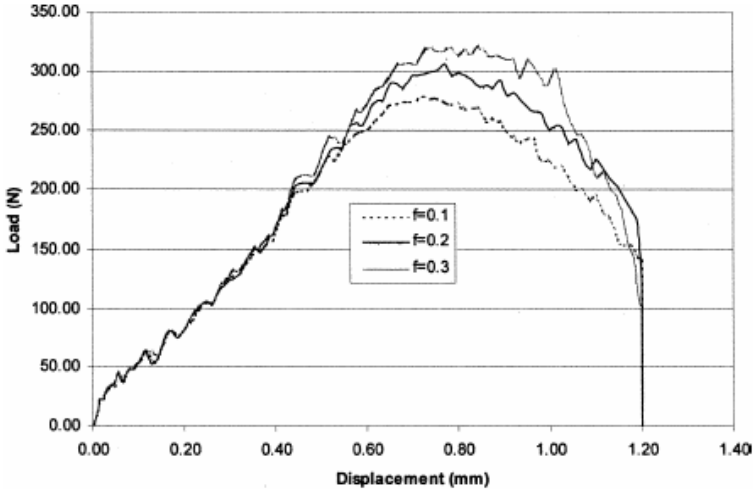

Fig. 3.4 Effect of the friction (Pathak et al., 2009)

From Fig. 3.2, it is seen that the punch head force is larger for the cases with friction coefficient than that without friction. This different is more significant at the final punch stage. That means that more work is required for the punch head to deform the sample disk when there is friction between the punch head and disk, which is

expected.

When the punch head displacement is from 0 to 1.0mm, the force needed does not differ much between the friction and frictionless cases. The deviation between the frictionless case and the case with coefficient of 0.05 can be as large as 10.8%, but it is as low as 3.0% for small punch displacements in the 0 to1.0mm range. At small deformations, the punch force and the contact area between the punch head and the disk are small such that little work is done by the frictional force. However, for large deformations, the contact area becomes large and the interaction of the punch head and the disk can no longer be ignored. This trend is in agreement with that reported by Pathak et al. (2009) (see Fig. 3.4).

Form Fig. 3.3, it is observed that the friction energy is much smaller than the total energy. This indicated that when the deformation is small, the friction effect can be ignored to simplify analysis when the specimen is well polished.

3.2 Sample Thickness

Specimen thickness is also an important parameter that influences the punch head force in a SPT. To study the effect of sample thickness, a FE model with the disk thickness of 0.45, 0.50mm, 0.55mm and 0.60 mm, respectively, is simulated (see Fig. 3.5). The fixed boundary conditions are used in the FE model.

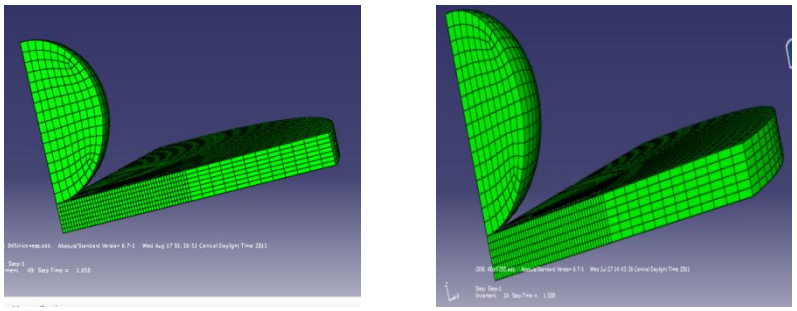

a. b.

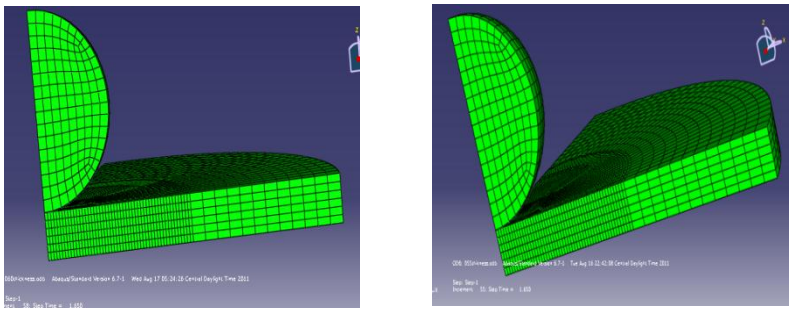

c. d.

Fig. 3. 5 Sample thickness effect FE model,
a. 0.45mm, b. 0.50mm, c. 0.55mm, d. 0.60mm.

The FE simulation results are plotted in Fig. 3.6.

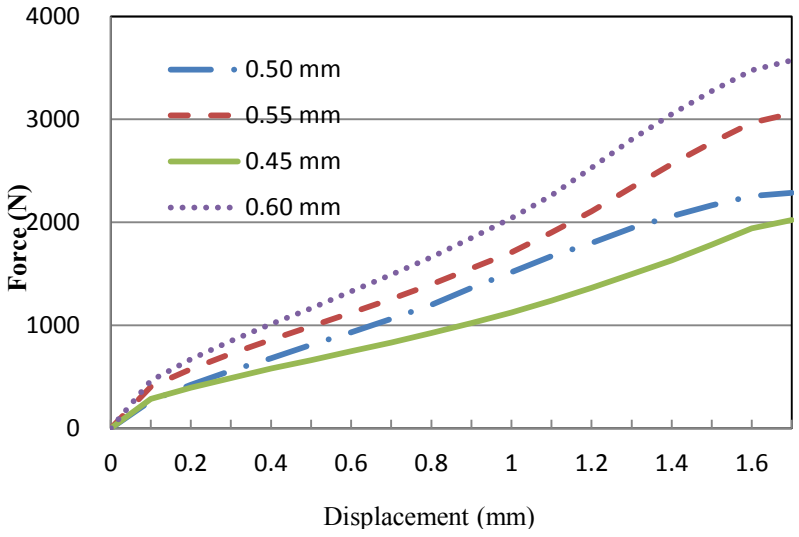

Fig. 3.6 Effect of the specimen thickness

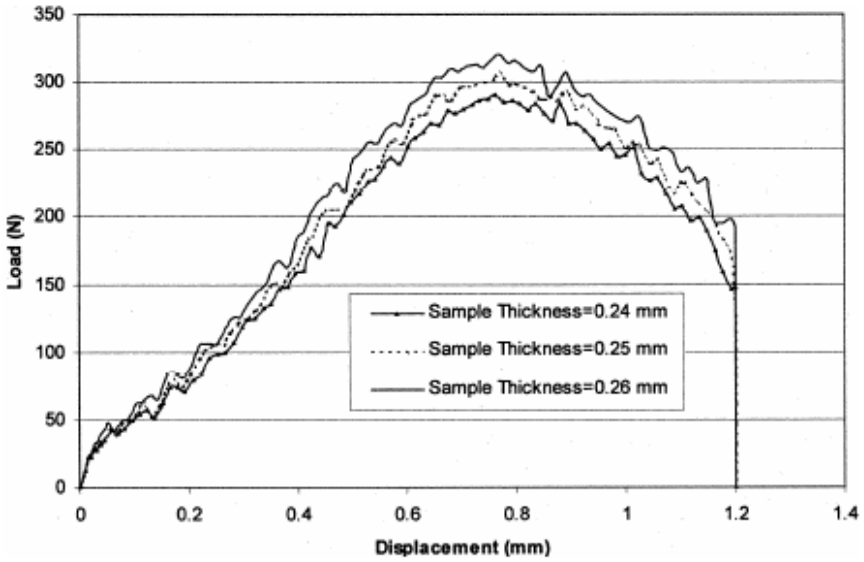

Fig. 3.7 Effect of sample thickness (Pathak et al., 2009)

It is seen from Fig. 3.6 that the sample thickness is a primary parameter that affect the punch head force. As thickness increase by 10%, punch head force is increased by 15~25%. This difference is more significant when the punch head displacement is large. However the relationship between the punch head force and the disk thickness is not linear, and as thicker specimen requires a much larger force to deform.

The trend shown in Fig. 3.6 is in agreement with that reported in Pathak et al. (2009) (see Fig. 3.7).

3.3 Punch Head Size

SPTs conducted using different experimental set-ups can lead to deviations in measured results. Punch head size is a primary parameter in a SPT, since different head size may result in variation of load-displacement curves. This size effect is analyzed

with the punch head radius being 1.0mm, 1.20mm and 1.25mm respectively (see Fig. 3.8).

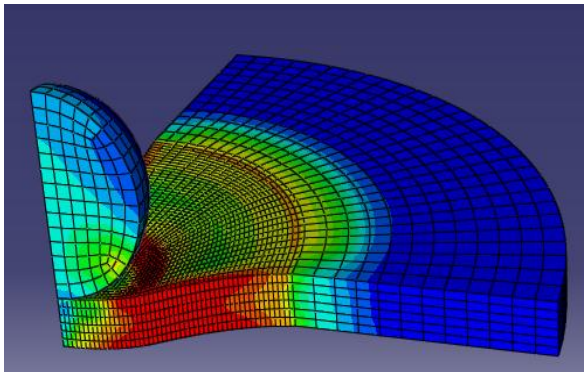

(a)

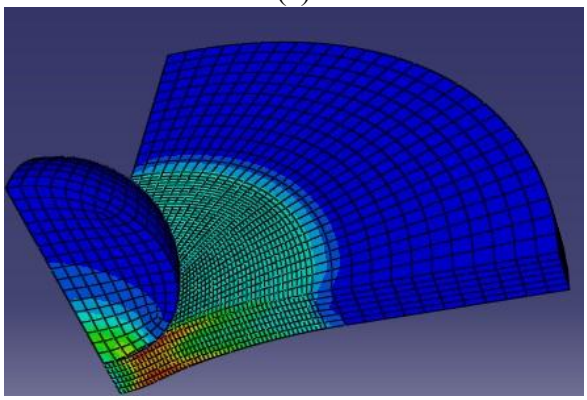

(b)

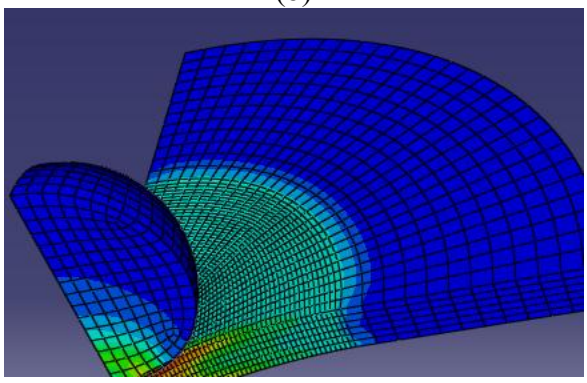

(c)

Fig. 3.8 Punch head size effect,
a. R = 1.0 mm, b. R = 1.2 mm, c. R = 1.25 mm

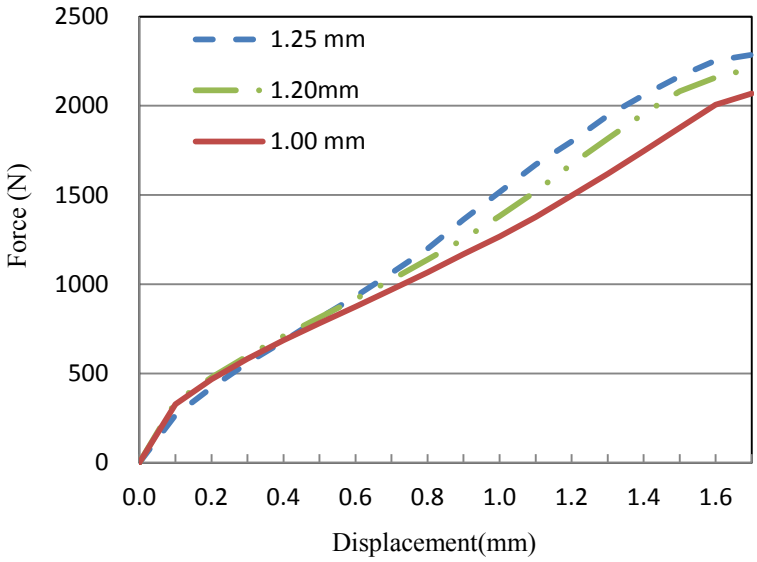

Fig. 3.9 FE simulation results for different punch head sizes effect

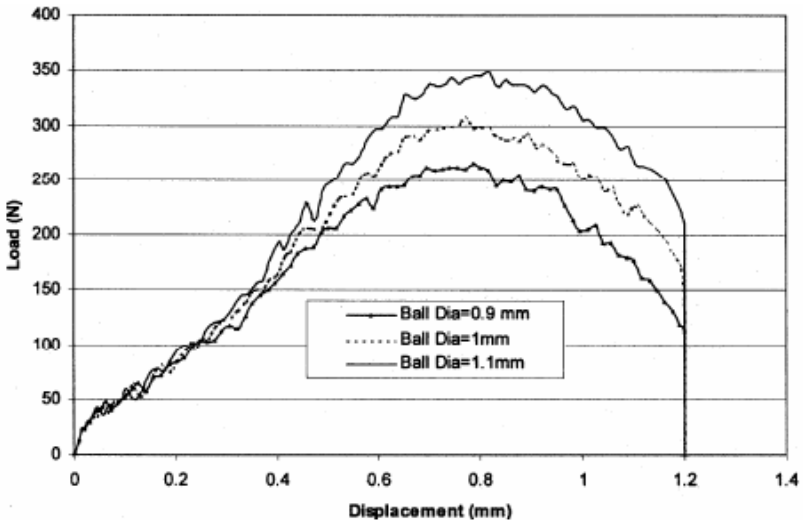

Fig. 3.10 Effect of the punch head ball diameter (Pathak et al., 2009)

The FE simulation results are shown in Fig. 3.9. At the beginning of the load-displacement curve, a smaller head requires a larger force to generate same punch head

displacement while may be due to the stress concentration effect. A smaller punch head will result in a larger stress concentration effect that requires larger force to deform disk. In the late stage of the deformation, a larger punch head corresponds to a larger force to produce same punch head displacement. This trend is in agreement with that observed in Pathak et al. (2009) (see Fig. 3.10).

3.4 Specimen Scale

Specimen scale is also an important parameter that affects the load-displacement curve. As shown in Fig. 3.11-3.12, the FE models are simulated using the ABAQUS CAE program with the disk thickness t = 0.25 mm, and the disk radius is 3mm and 1.5mm, respectively. The smaller specimen with r = 1.5 mm and t = 0.25 mm is suitable for the TEM use.

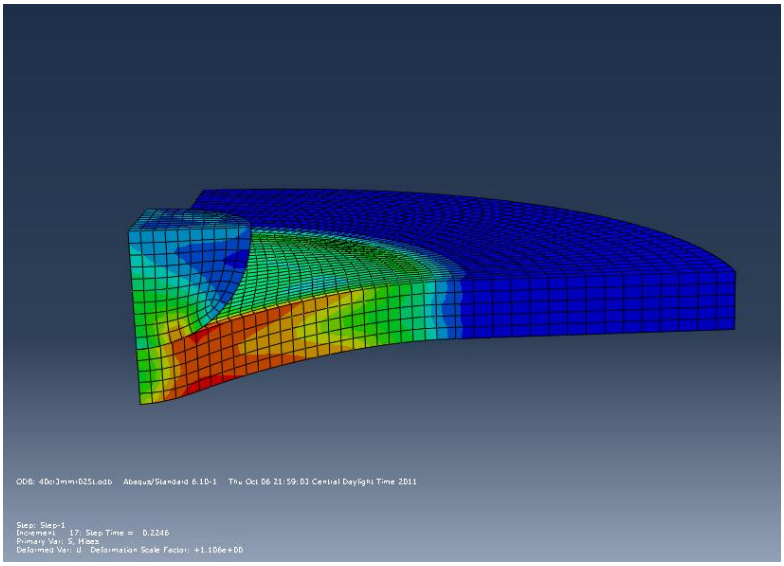

Fig. 3.11 FE Model with r = 3mm, t = 0.25 mm

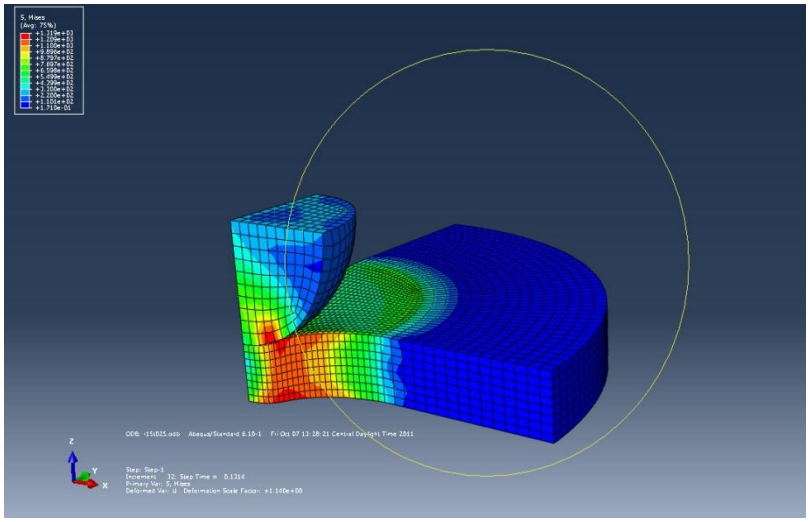

Fig. 3.12 FE Model with r = 1.5mm, t = 0.25mm

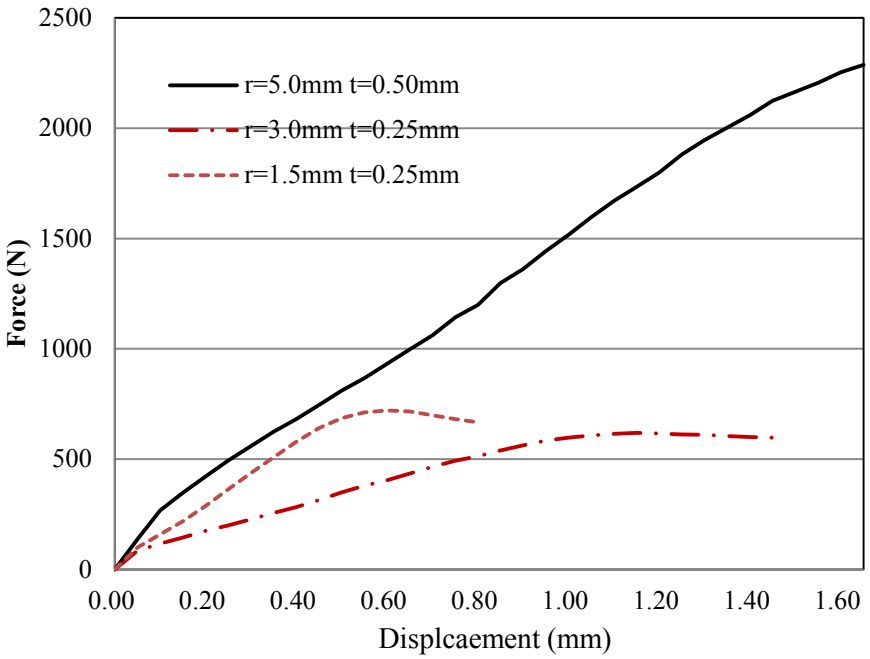

Fig. 3.13 Load-displacement curves for various scale model

The FE simulation results are shown in Fig. 3.13. It is seen that as the specimen size decreases in radius and thickness, the punch force decreases significantly. When compared with the SPT specimen with r = 5.0 mm and t = 0.5 mm used in Guan et al. (2011).

Fig. 3.13 also shows that when comparing the specimens with the same thickness 0.25mm and different radii 3.0mm and 1.5mm, punch force is larger for the specimen with the smaller radius. This suggests that the two specimens with the same thickness, the one with the smaller radius is stronger. This agrees with the general size effect observed for small components and devices.

3.5 Boundary Conditions

The FE simulations presented in Chapter II and so far in this chapter are based on a fixed model in which there is no slip between the holder and the specimen. However, in reality, disk may move a little bit even when it is held tight. This situation can be simulated using a FE model with the disk clamped by the holder, as shown in Fig. 3.14.

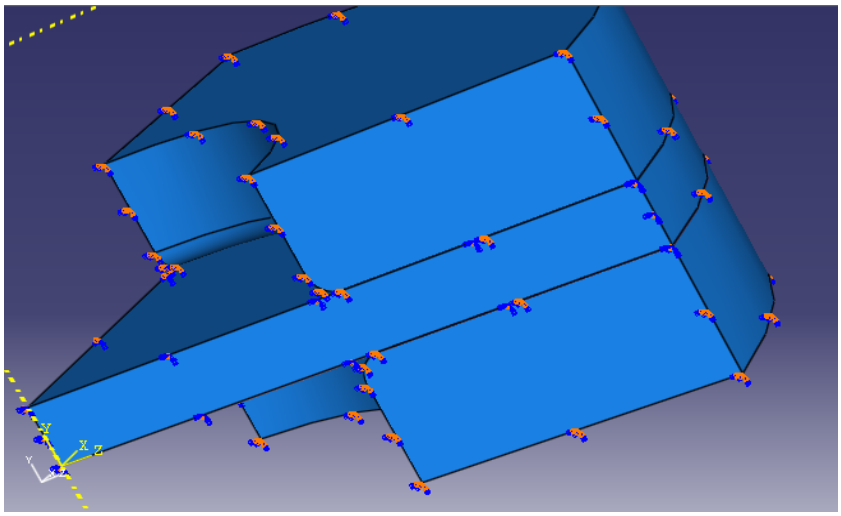

Fig. 3.14 Clamped boundary conditions

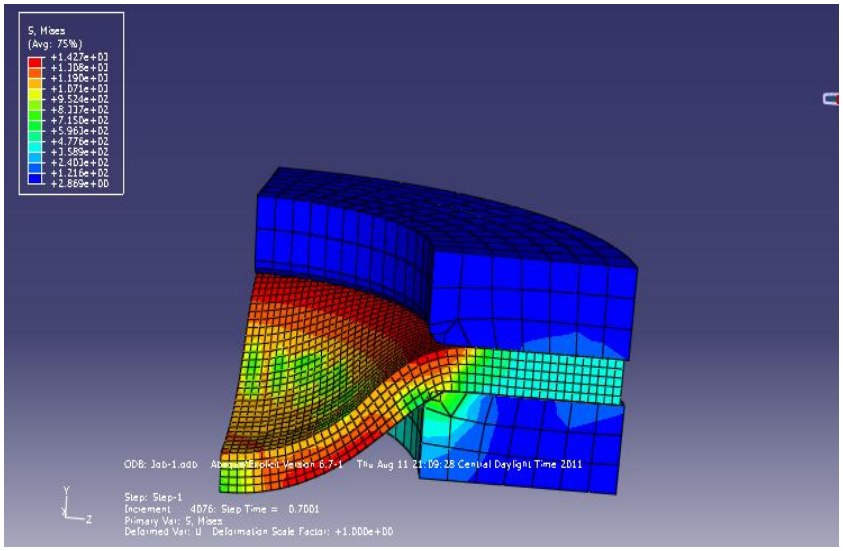

Fig. 3.15 Von-Mises stress distribution from the FE model with clamped boundary conditions

In Fig. 3.8., the boundary conditions for the disk is that $U_\theta=U_{rz}=U_{rr}= 0$, U_z, U_r and $U_{r\theta}$ are free. The friction coefficient between the punch head and the disk is 0, i.e., frictionless, in order to compare with the results obtained in the earlier simulations. Also,

there is no interacting force between the holder and the disk before punching starts.

The FE simulation results using the current clamped boundary conditions are shown in Fig. 3.15.

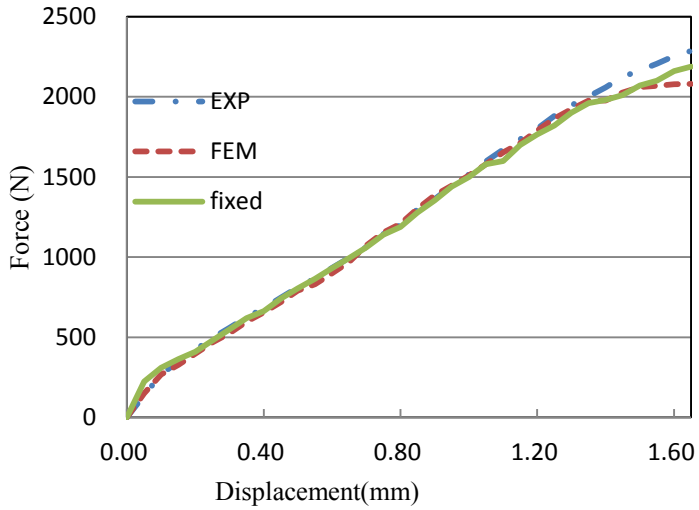

Fig. 3.16 FE simulation results with the clamped boundary conditions

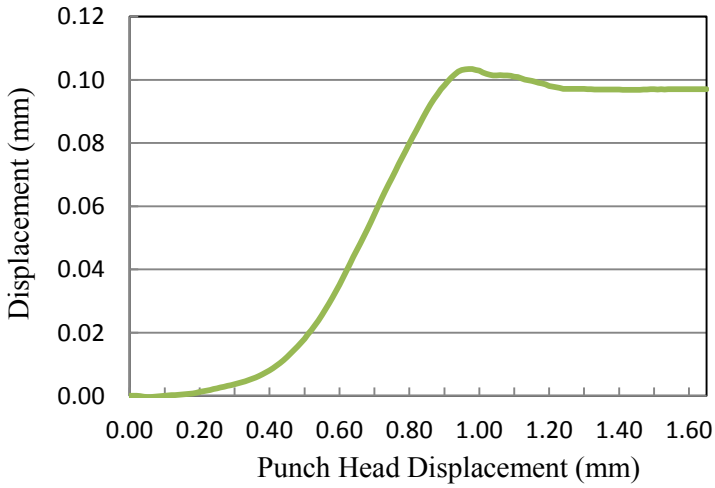

Fig. 3.17 Displacement of the disk in radical direction with the clamped boundary condition

It is seen from Fig. 3.16 that the resultant force from the model with the clamped boundary conditions is smaller than that with fixed boundary conditions. Fig. 3.17 shows the disk movement at radius 5 mm in the radical direction. The slip reaches over 0.1 mm, which is 2% of the radius, the movement is small initially and becomes large as the punch head displacement becomes large.

3.6 Summary

In a SPT, the load-displacement curve depends on several parameters. The effects of these parameters are studied in this chapter including friction coefficients, specimen thickness, specimen scale, punch head size, and boundary conditions.

The FE simulation results show that the friction coefficient and the boundary condition significantly affect the punch head only at large deformations. However, the specimen thickness and punch head size have significant effects on the punch force in all cases.

CHAPTER IV

CONCLUSION

Small punch test (SPT) is a widely used experimental technique to evaluate mechanical properties of in-service components together with a finite element analysis.

An improved inverse finite element method is proposed to characterize constitutive relations of materials based on the load-displacement curves from SPTs. This method enables the determination of the elastic modulus independent of the plastic properties, which improves the accuracy in characterizing the post-yield behavior of the material.

The effects of parameters including friction coefficient, specimen thickness, punch head size, specimen scale, and boundary conditions are analyzed in this study. The FE simulation results show that the friction coefficient and boundary conditions have less significant effects, while the specimen thickness and punch head size significantly affect the punch force.

Since the current research is a numerical study, the proposed inverse method can be validated with tensile tests in the future. More efforts should be focused on the standardization of experimental procedures to improve the efficiency in using SPTs.

REFERENCES

Aberdroth, M., Kuna, M., 2006. Identification of ductile damage and fracture parameters from the small punch test using neutral network. Engineering Fracture Mechanics 73, 710-725.

Baik, J.M., Buck, O., Kameda, J., 1986. Development of small punch test for ductile-brittle transition temperature measurement of temper embrittled Ni-Cr steel. *The use of small-scale specimens for testing irradiated material*. ASTM, Philadelphia, (USA).

Baik, J.M., Kameda, J. and Buck, O., 1983. Small punch test evaluation of inter-granular embrittlement of an alloy steel. Scripta Metallurgica 17: (12), 1443-1447.

Becker, A.A., Hyde, T.H., Xia, L., 1994. Numerical analysis of creep in components. The Journal of Strain Analysis for Engineering Design 29,185-192.

Bicego, V.， Lohr, R.D., 2000. Mechanical testing on miniature specimens by the small punch method. International Symposium on Materials Ageing and Life Management, Kalpakkam, India, Oct. 2000, 1445- 1454.

Bicego, V., Lucon, E.， Crudeli, R., 1995. Integrated technologies for life assessment of primary power plant components. Nuclear Engineering and Design 182, 113-121.

Bicego, V., Lucon, E., Crudeli, R., 1998. Integrated technologies for life assessment of primary power plant components. Journal of Nuclear Science and Engineeg 6 (2), 34-43.

Butt, P., Korzekwa, A., Maloy, A., Kung, H., Petrovic, J., 1996. Impression creep behavior of SiC particle-MoSi2 composites. Journal of Materials Research 11, 1528-1536.

Campitelli, E.N., Spatig, P., Bonade, R., Hoffelner, W., Victoria, M., 2004. Assessment of the constitutive properties from small ball punch test: experiment and modeling, Journal of Nuclear Materials 335, 366-378.

Chen, J., Ma, Y.W., Yoon, K.B., 2010. Finite element study for determination of material's creep parameters from small punch test. Journal of Mechanical Science and Technology 24 (6), 1195-1201.

Corwin, W.R., Lucas, G. E., 1986. *The use of small-scale specimens for testing irradiated material*. ASTM, Philadelphia, (USA).

Ding, K., Li, Y., 2009. Research status and prospects for small punch testing technique. Advanced in Mechanics 39, 299-315.

Dobes, F., Milicka, K., Ule B., Sustar, T., Bicego, V., et al., 1998. Miniaturized disk bend creep test of heat resistant steels at elevated temperatures. Engineering Mechanics 5 (3): 157-160.

Dooley, M., Lucas, G. E., and Sheckherd, J. W., 1981. Small scale ductility tests. Journal of Nuclear Materials 104, 1533-1537.

Dymacek, P., Milicka, K., 2008. Small punch testing and its numerical simulations under constant deflection force conditions. Strength of Materials 40, 24-27.

Egan, P., Whelan, M.P., Lakestani, F., Connelly, M.J., 2007. Small punch test: An approach to solve the inverse problem by deformation shape and finite element

optimization. Computational Materials Science 40, 33-39.

European Committee for Standardization (CEN), 2007. Small Punch Test Method for Metallic Materials Workshop 21.

Foulds, J., Viswanathan, R., 1994. Small punch testing for determining the material toughness of low alloy steel components in service. Journal of Engineering and Material Technology 116, 457-465.

Guan, K., Li, H., Wang, Q., Zou, X., Song, M., 2011. Assessment of toughness in long term service CrMo low alloy steel by fracture toughness and small punch test. Nuclear Engineering and Design 241, 1407-1413.

Gurson, A.L., 1977. Continuum theory of ductile rupture by void nucleation and growth: Part I-Yield Criteria and flow rules for porous ductile media, Journal of. Engineering Materials and Technology 99, 2-15.

Hu, R., Ling, X., 2009. Three-dimensional numerical simulation on plastic damage in small punch specimen of Zirconium. International Journal of Pressure Vessels and Piping 86, 813-817.

Huang, F.H., Hamilton, M.L., Wire, G.L., 1982. Bend testing for miniature disks. Nuclear Technology 57 (2), 234-242.

Husain, A., Sehgal, D.K., Pandey, R.K., 2002. Design of simple, versatile, small-specimen punch test setup for determination of the mechanical behavior of materials. Experimental Mechanics. 26, 33-38.

Husain, A., Sehgal, D.K., Pandey, R.K., 2004. An inverse finite element procedure for the determination of constitutive tensile behavior of materials using

miniature specimen. Computational Materials Science 31, 84-92.

Jerome, I., Akira, K., Kazuhiko, S., Tetsuo, S., 2008. Assessment of the Effects of Cold Work on Crack Initiation in a Light Water Environment Using the Small-Punch Test. Metallurgical and Materials Transactions A 39, 1099-1108.

Jung, P., Hishinuma, A., Lucas, G.E., Ullmaier, H., 1996. Recommendation of miniaturized techniques for mechanical testing of fusion materials in an intense neutron source. Journal of Nuclear Material 232, 186-205.

Lucas, G.E, 1990. Review of small specimen test techniques for irradiation testing. Metallurgical and Materials Transactions A 21, 1105-1119.

Lucas, G. E., Odette, G. R., Matsui, H., Moslang, A., Spaetig, P., Rensman, J., Yamamoto, T., 2007. The role of small specimen test technology in fusion materials development. Journal of Nuclear Materials 367, 1549-1556.

Lucas, G.E., Okada, A., and Kiritani, M., 1986. Parametric analysis of the disc bend test, Journal of Nuclear Materials 141-143 (1), 532-535.

Manahan, M.P., Argon, A.S., Harling, O.K., 1980. Alloy development for irradiation performance in fusion reactors. Annual Report, Sep.1979-Sep.1980 Massachusetts Institute of Technology, Cambridge, MA. Nuclear Reactor Lab.

Manahan, M.P., Argon, A.S. and Harling, O.K., 1981. The development of a miniaturized bend test for the determination of post irradiation mechanical properties. Journal of Nuclear Material. 104, 1545-1550.

Mao, X., Shoji, T., Takashashi, H., 1987. Characterization of fracture behavior in small punch test by combined recrystallization-etch method and rigid plastic analysis.

Journal of Test and Evaluation 15, 30-37.

Mao, X., Shoji, T., Takashashi, H., 1991a. Estimation of mechanical properties of irradiated nuclear pressure vessel steel by use of subsized CT specimen and small ball punch specimen. Scripta Metallurgica 25, 2487-2490.

Mao, X, Shoji, T, Takashashi, H., 1991b. Small punch test to predict ductile fracture toughness JIC and brittle fracture toughness KIC. Scripta Metallurgica 25, 2481-2485.

Milicka, K.， Dobeg, F., 2004. The high temperature characterization of welded joints using small punch testing. Materials and Technology (Material in Technologies) 38(1-2), 35-45.

Needleman, A., and Tvegaard, N., 1984. Analysis of the cup-cone fracture in a round tensile bar. Acta Metallurgica 32, 157-169.

Okada, A., Lucas, G.E., and Kiritani, M., 1988. Micro-bulge test and its application to neutron-irradiated metals. Transaction of the Japan Institute of Metals 29, 99-108.

Parker, J.D., Stratford, G.C., Shaw, N., Spingk, G., Tate, E., Conroy, R.D., et al. 1995, Deformation and fracture processes in miniature disc tests of CrMoV rotor steel. Third International Charles Parsons Turbine Conference, Newcastle (UK).

Pathak, K., Dwivedi, K., Shukla, M., Ramadasan, E., 2009. Influence of key test parameters on SPT results. Indian Journal of Engineering and Materials Sciences 16, 385-389.

Schwant, C., Timo, P., 1985. Life assessment of general electric large steam

turbine rotots. *Life Assessment and Improvement of Turbo-Generator Rotors for Fossil Plants*, NewYork, USA, Sep. 1984, 3.25-3.40.

Takahashi, H., Shoji, T., Mao, X., Hamaguchi, Y., Misawa, T., Saito, M., Oku, T., Kodaira, T., Fukaya, K., Nishi, H., and Suzuki, M., 1988. Recommended practice for small punch (SP) testing of metallic materials, Japan Atomic Energy Research Institute M, 88-172.

Tvergaard, N., 1981. Influence of voids on shear band instabilities under plane strain conditions. International Journal of Fracture 17, 389-407.

Zhou, Z., Zheng, Y.Z., Ling, X., Hu, R., Zhou, J., 2010. A study on influence factore of small punch creep test by experimental investigation and finite element analysis. Material Science and Engineering A 527, 2784-2789.

VITA

Ms. Zhenzhen Xu received her Bachelor of Science in Engineering Mechanics from Central South University in Changsha, China in 2003. She entered the Department of Mechanical Engineering at Texas A&M University in September 2008 and received her Master of Science degree in December 2011. Her research interests include solid mechanics, finite element analysis and structural engineering.

Ms. Xu may be reached at Ms. Xu, c/o Dr. Gao, Department of Mechanical Engineering, Texas A&M University, 3123 TAMU, College Station TX 77843-3123. Her email is xuzhenzhentamu@gmail.com.